Subscale Rotor Spin Testing for Compulsator Component Development

K. G. Cook, B. T. Murphy, S. M. Manifold, T. Pak,
M. D. Werst, J. R. Kitzmiller, and W. A. Walls
Center for Electromechanics, The University of Texas at Austin

A. Alexander and K. Twigg
Custom Analytical Engineering Systems

Abstract —The maturation of pulsed rotating machines has evolved to the stage where a greater degree of basic research is required to further increase the energy and power density of advanced compulsators. The University of Texas at Austin Center for Electromechanics is studying the combined mechanical and electrical aspects of very high speed compulsator rotor designs for the next generation of compact pulsed rotating machines.

This paper describes the design, construction, and testing of three scaled composite rotors. Performance specifications included hoop stresses of 1.7 GPa (250 ksi) in the outer banding and strain excursions of 0.4% in the field coil region. Results from the three studies are reviewed in detail. Techniques developed at the Center for Electromechanics for determining composite rotor performance are also discussed.

INTRODUCTION

The University of Texas at Austin Center for Electromechanics (UT-CEM) pursues leadership in pulsed power technology through the development of high speed rotating electrical machines. To date, these machines have been designed to operate at hoop stresses of 1.2 GPa (175 ksi). UT-CEM was contracted to perform a series of tests using scaled test rotors to explore the next level of operating regimes. These tests were to establish hoop strain capabilities in field windings and composite banding performance up to 1.7 GPa (250 ksi) hoop stress levels.

The experimental study was approached in incremental test series. Series I tests focused on a flexible arbor design to allow testing of future candidate coils, banding combinations, and field coil insulation durability. Series II testing provided an increased focus on testing at intermediate coil strain and banding stress levels. The third series increased both field coil hoop strains and the hoop stresses in the outer banding over those in series II. Throughout the program, axisymmetric finite element models were maintained to reflect as-built dimensions of each rotor and used to predict rotor behavior during spin testing. To date, three coil/banding configurations have been designed, built, and tested. Table 1 provides nominal design criteria for each of the test series.

Manuscript received May 1, 1998.

K.G. Cook may be reached at 512-471-4496, fax 512-471-0781, k.cook@mail.utexas.edu.

This work was supported by The University of Texas Institute for Advanced Technology under contract no. DAAA21-93-C-0101.

Table 1. Summary of rotor design and performance criteria.

Test Series	Field Coil Design	Speed (rpm)	Field Coil Strain	Banding Hoop Stress (GPa)	(ksi)
I	Single Layer	18,500	0.2%	0.3	48
IIA	Double Layer	24,300	0.2%	1.2	175
IIB	Double Layer	33,500	0.4%	1.7	250

SERIES IA

Design

Rotor IA went into production with the intent to study composite banding hoop strength. Because of milestone achievements in other programs [1][2], it became apparent that more knowledge could be gained in rotor technology if the focus was adjusted toward the durability of composite electrical structures that have been repeatedly strained. The objectives of series IA became designing a coil/banding that could maintain interface pressure while experiencing a hoop strain of 0.2% in the active region of a field coil and to develop an arbor/rotor for future spin tests.

Once banding hoop strength was no longer the issue, the most challenging aspect of the project was designing the means of connecting the rim to the testing facility's drive shaft. Connecting the rim to the shaft via a solid disk structure was unsuitable due to the large amount of interference at the disk-to-rim interface required to prevent separation at high rotational speeds. Achieving the amount of interference needed would have been difficult, if not impossible, and the radial precompression at rest would have been high enough to accelerate the viscoelastic response of the composite bandings and field coil matrix, resulting in a possible loss of precompression with time.

A conceptual design for a conical shaped spin test arbor constructed of high strength steel was developed and analyzed via one-dimensional (1-D) axisymmetric nested ring analysis and two-dimensional (2-D) axisymmetric finite element analysis.[4] The conical shape is compliant compared to a solid disk, allowing growth-matching of the arbor with the rim. This greatly reduces the need for a large interference fit and results in significantly reduced radial precompression at rest as well.

The spin test arbor was designed to allow testing of a scale representation of an active region slice of a sample rotor. Design goals for the arbor included:

- Capability of operation to stresses of 1.7 GPa (250 ksi)
- Re-usability
- Ease of fabrication

Based on the results of initial analysis, a 2-D axisymmetric finite element model was constructed using PATRAN 2.5 software. The arbor, the intermediate bandings, and a representation of the test rim were modeled. Interface elements were used to model S-glass banding interferences and the test rim interference. No attempt was made to model the individual components of the test rim or their interferences. Rather a representative rim was modeled that was tuned to provide the same average stiffness and density as the test rim. The arbor, S-glass bandings and the test rim were all modeled with a 0.2° taper angle. Four cases were run, corresponding to loading conditions due to interference only at 0 rpm, and interference and spin loading at 40,000 rpm, 42,000 rpm and 43,860 rpm.

Although there is a significant amount of bending in the arbor at 0 rpm, the von Mises stress is less than 1.0 GPa (145 ksi). At 40,000 rpm, the von Mises stress increased to 1.2 GPa (180 ksi), 1.4 GPa (209 ksi) at 42,000 rpm and 1.6 GPa (239 ksi) at 43,860 rpm. These values compare very well to the hoop stresses calculated in the nested rings analysis, indicating that in all cases the hoop stress is the significant component of the von Mises stress.

Radial stresses in the S-glass banding at the end of the arbor compare favorably with those predicted by nested rings analysis. At the other end, however, there is a substantial deviation due to the increased stiffness of the cone of the arbor. This radial tension buildup is due to the end of the S-glass banding and test rim losing contact with the arbor as the arbor deflects. To ensure radial compression throughout the bandings up to 43,860 rpm, the interference was increased slightly. Axial and RZ shear stresses in the bandings are low compared to the material strength, as are hoop stresses in the S-glass bandings.

Rotor IA was also analyzed for its rotordynamic characteristics. During spin testing, the rotor was suspended vertically in a pendulum fashion from a 9.5 mm (0.375 in.) diameter quill shaft, within a spin test pit. For successful spin pit testing, two rotordynamic conditions must be satisfied; 1) the first flexible bending mode frequency of the test rotor must be at least 20% above the maximum spin test speed, and 2) the rigid rotor conical mode frequency should be at least 20% above or below the rotor speed for all speeds up to the maximum spin test speed. All configurations analyzed satisfied these two requirements. Maximum margins were obtained with a steel arbor with a hub having a short axial length.

Testing

The IA test rotor was spun successfully six times up to a planned maximum speed of 18,500 rpm. The key result of the tests was that the dynamic performance of the rotor was consistent and showed no significant variation from test to test. This is important because it means that any movement or shifting of material within the rotor, if any occurred, did not affect the high precision balance of the rotor.

Rotor deflection data was acquired during each test from four eddy current proximeter probes and two laser probes. This is the first attempt at UT-CEM to use laser probes to measure deflection of a composite high speed rotor surface.[4] Fig. 1 shows the arrangement of the probes. The laser probe labeled "Aromat" was reading off a graphite surface. All other probes were reading off the surface of the 4340 steel arbor. In the arrangement shown, the proximeter probe labeled "Bore" was to serve as a reference against which the two laser probes would be compared. The initial findings with the laser devices were encouraging, but not conclusive. For this reason, the data is not included in this paper.

The manageable size of rotor IA lent itself to exploring new destructive and non-destructive techniques for evaluating the performance of a rotor spun at a high velocity. A CAT scan attempt did not provide any usable data due to interference from the steel arbor and steel rim in addition to the inadequate resolution capabilities of the equipment.

15X and 45X micrographs of the field coil end planes were nearly indistinguishable in their pre- and post-spin appearance. The Teflon tape pulled away from the conductor in some instances, but this appears to be related to surface preparation. No evidence of crazing or cracking in the post-spun field coil could be seen.

In order to study the interior of the rotor, three 1.27 cm (0.5 in.) thick rings were parted from the test rotor for examination. This was the first time that a highly prestressed rotor had been disassembled in this manner by UT-CEM. After close inspection, no spin induced damage was observed in the bandings or the field coil of rotor IA.

Series IIA

Design

Rotor IIA was configured to verify the structural adequacy of a representative field coil under anticipated operating conditions including strain excursions of 0.2% and high voltage insulation capabilities.[3] The field coil configuration incorporated in rotor IIA is representative of the conductors, insulation, and race track geometry utilized in full scale machines. A key tech-

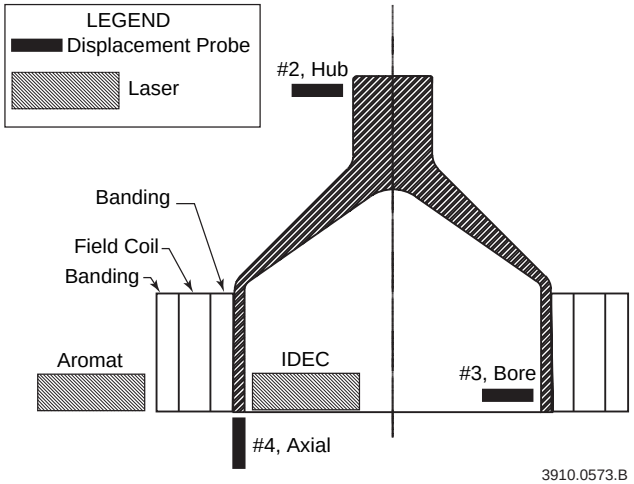

Fig. 1. Rotor IA instrumentation location.

nical issue with this type of design involves structural adequacy of the field coil conductor insulation to sustain induced transverse strains arising from rotor growth during spin up from the at-rest condition to design rotational speed. In the rotor's at-rest condition, the sequential build-up of bandings using interference fits results in radial compressive stresses that induce hoop compression in the field coil region corresponding to transverse compressive strains in the conductor insulators. Radial growth induced in the rotor during spin up subsequently superimposes hoop tensile loads on the field coil resulting in average transverse tensile strain excursions of 0.4% in the conductor insulators. Since the transverse stiffness of insulation is two orders of magnitude less than the stiffness of the aluminum conductors, these average transverse tensile strains are primarily absorbed by the insulation material between conductors, resulting in significantly higher transverse strains induced in the insulation.

The rotor IIA design was configured to reflect conditions on the field coil in both the at-rest and the at-spin states. It was also desired that construction of rotor IIA would be representative of the sequential interference fit assembly procedures typically incorporated in this type of rotor configuration.

The 2-D detailed axisymmetric finite element model of the rotor is shown in Fig. 2. Surface interactions between the components were modeled using non-linear interface elements and axial constraints to simulate bonding. Material properties for the composite rings were generated using a CAES proprietary pre-processor. The pre-processor uses the ply-by-ply lay-up and generates orthotropic material properties for each element based on the content of layers within that element. Properties for the field coil were calculated from results of testing done at UT-CEM on potted field coil sections. A double layer field coil section was modeled in detail. The aluminum conductor/insulation sections were modeled using the data measured by UT-CEM which was run through the CAES pre-processor to generate consistent orthotropic material properties. The insulation above and between coil layers, along with the glass cloth creating the tapers on the inside and outside of the field coil section were modeled separately.

Predicted average compressive hoop strains resulting from the assembly sequence and press fits are -0.2% in the inner field coil and -0.28% in the outer field coil (Fig. 3). The total transverse tensile strain excursion from the rest state to spin conditions at 24,000 rpm is 0.37% in the inner field coil and 0.36% in the outer field coil. Radial growth predicted by the finite element model is 4.7% higher than the corresponding measured values obtained from spin testing of the rotor. This reflects good correlation between the finite element model and the test data, as seen in Table 2.

Testing

The field windings were voltage tested during each phase of their construction. The first test, at 2 kV, was performed after Limitrak was applied to the coils. The second round of higher voltage testing was performed after the half-lapped layers of Teflon tape and glass tape were applied and after the coils had been assembled into a potted structure. The final tests were performed after the B2 banding was pressed into place over the Randolite layer and after each spin test was performed.

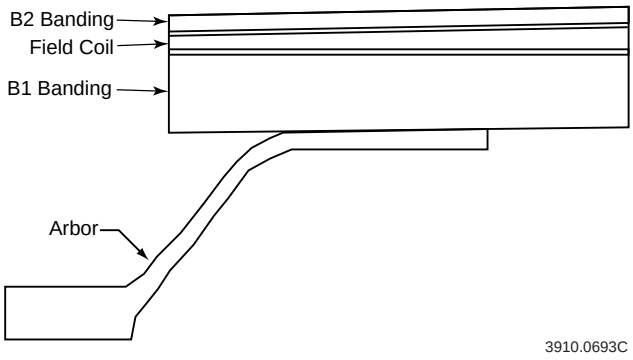

Fig. 2. Axisymmetric model of rotor IIA.

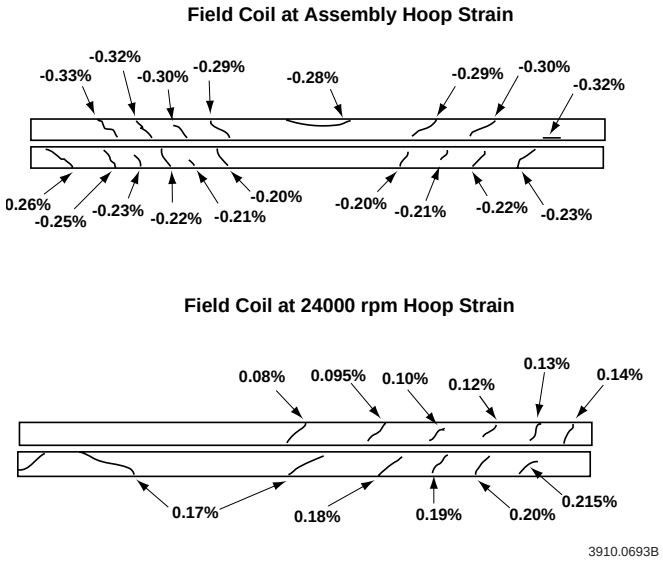

Fig. 3. Predicted hoop strain in rotor IIA.

Throughout manufacture and testing, the resistance was consistently measured in the gigaohm range.

The series IIA rotor was test spun in a vertical configuration inside the same air-turbine driven spin pit used for testing series IA. Two eddy current sensors were located on the ID of the steel arbor with one IDEC laser sensor on the graphite banding outer surface. The three sensors are non-contacting gap sensors. The two eddy current displacement sensors (Bentley Nevada) have a frequency response from dc to over 5,000 Hz. The laser displacement sensor made by IDEC (model MXIA-B12R6S) also measures gaps, in this case from 30 to 50 mm. This model laser sensor has a frequency response from dc to about 1 kHz. The laser has the key advantage of being able to read off non-conductive surfaces. The composite outer banding made with graphite has some conductivity, but not enough to produce an adequate signal with any of the eddy current sensors which were tried (including 5, 8, 14, 25 and 50 mm tip Bentley Nevada sensors).

Table 2. Measured and predicted growth values for rotor IIA

	Composite Rim			
	Measured		Predicted	
	(mm)	(in.×10^{-3})	(mm)	(in.×10^{-3})
Test 1	0.441	17.36	0.43	16.81
Test 2	0.452	17.78	0.43	16.81
Test 3	0.448	17.62	0.43	16.81
Test 4	0.452	17.79	0.43	16.81
Test 5	0.451	17.74	0.43	16.81
Test 6	0.446	17.56	0.43	16.81
Average	0.448	17.64	0.43	16.81
Std Dev	0.004	0.17		

Since the sensors can measure the dc component of the gap, they can measure the centrifugal growth of the rotor as well as any static lateral offset which occurs during a test. The two eddy current sensors are mounted 180° from each other. This makes it possible to distinguish dc gap changes due to centrifugal growth from that due to rotor lateral offset. The exact position of the rotor can change slightly as it spins up, making it necessary to measure this offset so that the rotor growth can be determined. The laser sensor was mounted in the same plane as the two eddy current sensors and will see the same offset.

The rotor was accelerated six times from rest to a planned maximum speed of 24,300 rpm. Dynamic gap data was acquired with a computer based multi-channel data acquisition system at a constant sample rate of 2,560 samples per second, per channel. This is adequate to measure analog frequencies up to about 1 kHz. Fig. 4 shows plots of the dc gap versus rotor rpm for test number 6. The anticipated quadratic nature of the data is clearly evident. As mentioned above, the gaps from the opposing eddy current sensors are used to determine the growth and offset ([s1+s2]/2 and [s1-s2]/2) of the steel hub. The offset is then used with rim gap data to determine the growth of the composite rim. Table 2 summarizes the measured and predicted growth values for all 6 tests.

The three sensors also measure the dynamic motion of the rotor. Fig. 5 shows the filtered synchronous vibration component for test #6. It is equivalent to the amplitude of the signal passed by a narrow bandpass tracking filter centered at the running speed frequency. The amplitude of this signal consists of the characteristic runout (i.e., waviness) of the target shaft surface, and synchronous whirling vibration motion of the rotor. The eddy current sensor amplitude is seen to level off at high speed at 0.03 mm (1.3 mils) radial peak amplitude. This means that the mass center of the rotor is radially displaced about 0.03 mm (1.3 mils) from the geometric centerline of the bore of the steel hub. By contrast the mass center is seen to be displaced about 0.05 mm (1.9 mils) peak from the geometric center of the outer composite rim. The centerlines of the hub and rim as indicated by their respective sensors are not coincident, but are offset about 0.02 mm (0.6 mils) from one another.

In Fig. 5, the trace of the rim amplitude begins to increase at 18,500 rpm. This behavior was duplicated in each of the six tests. There is no such change in behavior noted in the hub amplitude, implying that the balance of the rotor is not changing. It is believed that the indicated change in the rim amplitude is due to changes in the runout profile of the rim. As the centrifugal forces increase, any bulging out of the rim surface could manifest itself in precisely this manner. Amplitudes of the higher harmonics from the laser sensor are band limited by virtue of its 1 kHz maximum frequency output. Only the second harmonic could be monitored to speeds above 18,500 rpm. The second harmonic amplitude is around 0.01 mm (1.4 mils) peak, and only minor changes in amplitude were noted.

Rotor IIA met all of its design objectives. It achieved a hoop strain in the field coils of 0.2% while maintaining insulation integrity after spinning six times to 24,300 rpm.

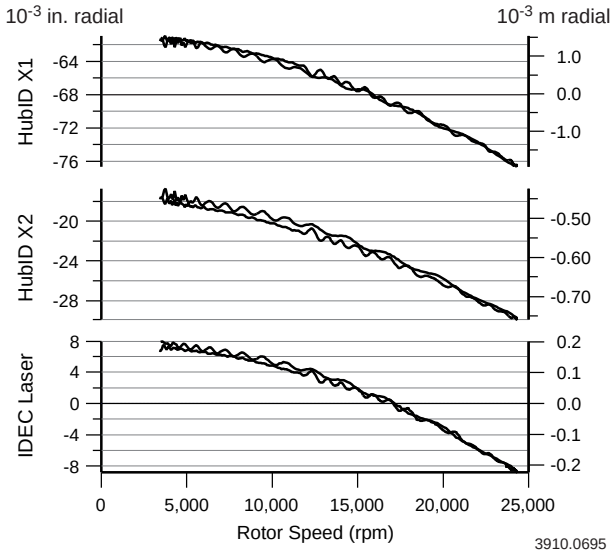

Fig. 4. Rotor IIA, run 6 growth vs. rotor speed.

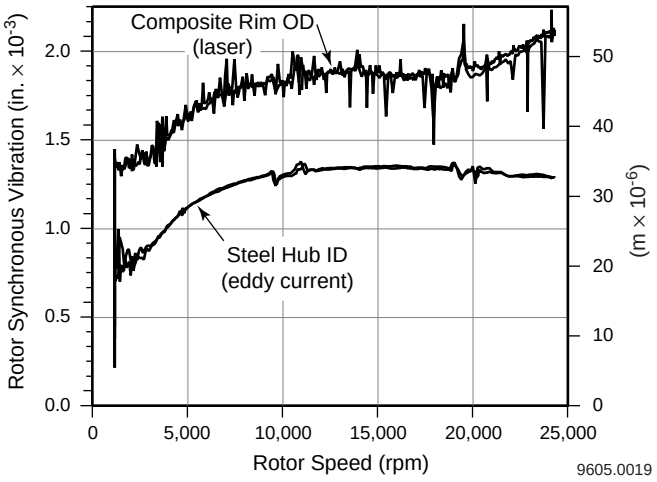

Fig. 5. Rotor synchronous vibration vs. rotor speed.

SERIES IIB

Design

The goals of this test series were to achieve a hoop stress of approximately 1.7 GPa (250 ksi) in the B3 banding and hoop strains of 0.4% in the field windings while maintaining radial compression in the rotor. To accomplish these goals, an additional banding (B3) was added to rotor IIA to allow it to reach higher tip speeds while maintaining radial compression. Secondary design issues that emerged during preliminary investigations involve maintaining stresses in the arbor below yield during assembly and minimizing the press load required to assemble the B3 banding.

Version IIB of the rotor represents a significant increase in stored energy and complexity in comparison to the IIA rotor. This is due not only to the fact that the IIB rotor has additional components, but also to the fact that its operating speed is 40% higher. Preliminary finite element analyses revealed that the IIA rotor–and, in particular, the steel arbor–had a high likelihood of failure if it was converted to IIB without modification. The main problem was the addition of the B3 banding required in the IIB specifications would have increased the at-rest compressive hoop stresses in the arbor above yield. It was concluded that a sleeve must be added to the inside diameter of the arbor to relieve these stresses.

The cross-section of the IIB rotor is given in Fig. 6. Once the IIB rotor design was determined, finite element analyses were undertaken in order to verify the performance criteria could be attained and also to help make salutary adjustments to the design. Due to the rotational symmetry of the rotor, a 2-D model was developed using axisymmetric finite elements.

Four analyses were performed on the IIB rotor. The first examined the effect of tapering the bore of the arbor to facilitate insertion of the sleeve without any of the IIB components (i.e., B3 and the support sleeve). The second analysis examined the effect of inserting the support sleeve into the tapered arbor bore, prior to assembly of the B3 banding. The final two analyses examined the full IIB rotor (with all components) in the at-rest and at-speed states.

The first analysis confirmed that there will be an inward deflection of the arbor ID of approximately 0.1°, producing a net taper angle of 0.5°. The analysis also showed that there will be a negligible increase ≈27.5 MPa (4 ksi) in arbor hoop stress due to the tapering. The second analysis confirmed that there will be significant reductions ≈172 MPa (25 ksi) in both arbor hoop stress and von Mises stress after insertion of the support sleeve. The analysis also showed that there will be a reduction in maximum radial displacement in the arbor of approximately 0.13 mm (0.005 in.).

The third analysis examined the full IIB rotor at rest. It verified that even after the outer loading bands have been assembled, the von Mises stress in the arbor should not exceed approximately 1.2 GPa (170 ksi), well below yield. The final analysis examined the full IIB rotor at a speed of 3,570 rad/s. It verified that the B3 banding should experience a maximum hoop stress of approximately 1.8 GPa (260 ksi), and the field coil should experience a maximum hoop strain of approximately 0.46%, as desired.

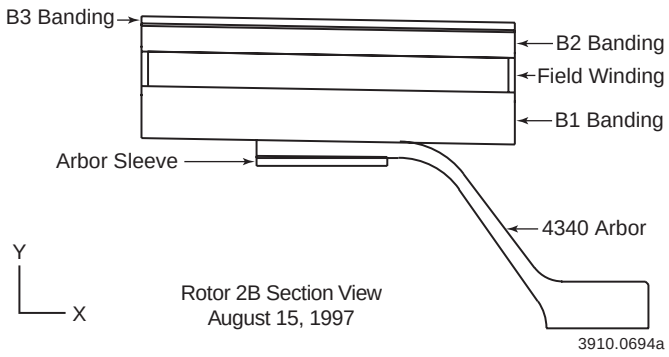

Fig. 6. Test rotor IIB section view.

The results of the finite element analyses were compared with closed-form solutions at the rotor midplane obtained by nested ring analysis and were in good agreement, except for the arbor. This was not unexpected since it is the arbor that deviates most from an ideal ring geometry.

Testing

As with the first two rotors, rotor IIB was also suspended from a spindle for spin testing. Provisions had been made with this rotor for hi-potting it between each run. Rotor IIB was successfully hi-potted after each spin test at the facility, then retested upon its return to UT-CEM where higher capacity equipment was available.

Instrumentation for rotor IIB was the same as for rotor IIA with one addition. A second IDEC laser sensor was installed 180° opposite the first. This allows a more direct measurement of the growth and offset of the outer surface of the rotor. A series of six test runs were conducted up to the planned speed of 33,500 rpm. Before testing, rotor IIB was balanced on a commercial balance machine to a mass center offset of less than 2.5×10^{-3} mm (0.1 mils). This offset is of the rotor mass center with respect to outer diameter of the steel hub at the point of quill shaft insertion. The rotor was supported in the balance machine by clamping onto the steel hub at this location.

Fig. 7 shows the growth from one of the IDECs for the last three tests. The shift in the data from test 4 to test 5 is from bumping the sensor mounting bracket a few millimeters while hipotting the rotor between runs. This has no affect on the growth measurements. Table 3 shows a summary of the measured and predicted growth for rotor IIB. The growth was underpredicted by 2.0×10^{-2} mm (0.8 mils), or 2.6%. Such close agreement helps verify that predicted strains, and thereby stresses, are computed with similar accuracy.

Fig. 8 shows the filtered synchronous vibration from the last test of rotor IIB. Traces from the five other tests were virtually identical. The vibration amplitudes again show the rotor balance to be retained throughout the test speed range for all tests. At high speed the downward drift in amplitude on the laser sensor is not accompanied by a significant change on the Hub ID sensor. These data indicate that the precision balance is not changing.

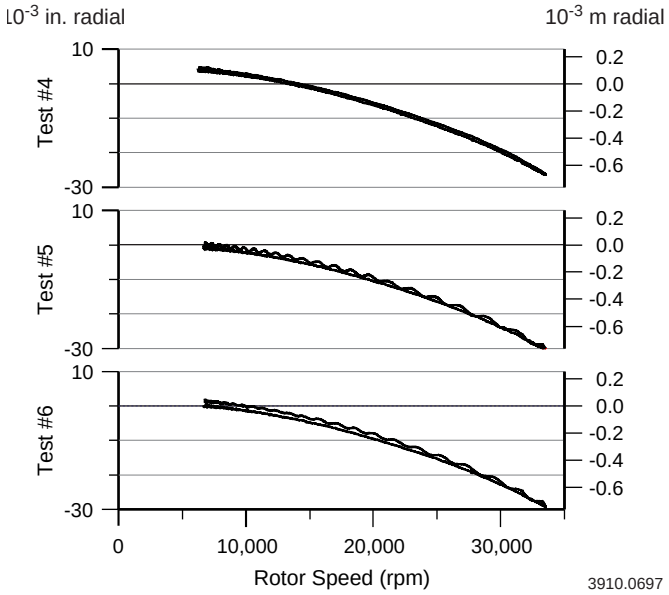

Fig. 7. Test rotor IIB OD growth.

Conclusions

Nested ring and axisymmetric finite element analysis of composite flywheels have become very reliable tools to predict behavior during high speed operation. Not only will they accurately predict rotor growth, they are invaluable in the design of each composite layer. Through the use of these tools, this program successfully reached each of its design goals, most of which had never been attempted before in the development of compulsators.

- Banding hoop stress of 1.7 GPa (250 ksi)
- Field winding strain excursions of 0.4%
- Development of high performance field winding insulation

The design and testing of these rotors, has demonstrated that the next generation of compulsators are based upon reliable engineering design. Continuing component research of this type will increase this reliability.

Acknowledgments

The authors would like to give a special thanks to all of the craftsmen who assembled these fine rotors, especially Mr. Richard Rodriguez.

Table 3. Filtered synchronous vibration of rotor IIB (data not yet reduced for tests 1,2,3)

	Composite Rim			
	Measured		Predicted	
	(mm)	(in.×10^{-3})	(mm)	(in.×10^{-3})
Test 4	0.77	30.44	0.79	31.020
Test 5	0.76	30.10	0.79	31.020
Test 6	0.77	30.16	0.79	31.020
Average	0.77	30.23	0.79	31.020
Std Dev	0.005	0.18		

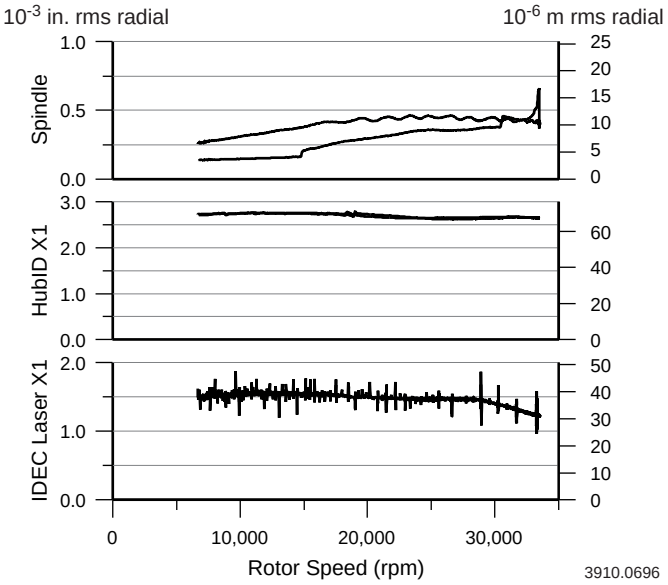

Fig. 8. Rotor IIB synchronous vibration vs. rotor speed.

References

[1] R.C. Thompson, “Report on burst spin test #1,” Test Devices Test Number C-2045, September 1996.

[2] R.C. Thompson, “Report on containment UT-CEM test #17,” Test Devices Test Number CEMB ZD-10, DARPA Flywheel Safety Program, November 18, 1997.

[3] J.J. Hahne, “High strain insulation systems for CPA rotors,” 9th EML Symposium, Edinburgh, Scotland, May 1998.

[4] K. G. Cook, “Development of compulsator rotor technology”, RF 163, Annual Technical Report for the Period of October 1996 to December 1996, presented to Ian McNab, IAT, August 1997.